

Supplementary information

Tailoring cobalt spinel oxide with site-specific single atom incorporation for high-performance electrocatalysis

Kangjae Lee^{1,2,7}, Jaehyuk Shim^{1,2,7}, Hyunsoo Ji^{1,2,7}, Jungho Kim⁶, Hyeon Seok Lee^{1,2},
Heejong Shin^{1,2}, Megalamane S. Bootharaju^{1,2}, Kug-Seung Lee³, Wonjae Ko^{1,2}, Jaewoo
Lee^{1,2}, Kang Kim^{1,2}, Seungwoo Yoo^{1,2}, Sungeun Heo^{1,2}, Jaeyune Ryu^{1,2}, Seoin Back^{6,*},
Byoung-Hoon Lee^{4,5,*}, Yung-Eun Sung^{1,2,*}, and Taeghwan Hyeon^{1,2,*}

¹*Center for Nanoparticle Research, Institute for Basic Science (IBS), Seoul 08826, Republic of Korea*

²*School of Chemical and Biological Engineering, and Institute of Chemical Processes, Seoul National University, Seoul 08826, Republic of Korea*

³*Pohang Accelerator Laboratory (PAL), Pohang University of Science and Technology (POSTECH), Pohang, Republic of Korea*

⁴*KU-KIST Graduate School of Converging Science and Technology, Korea University, Seoul 02481, Republic of Korea*

⁵*Department of Integrative Energy Engineering, College of Engineering, Korea University, Seoul 02481, Republic of Korea*

⁶*Department of Chemical and Biomolecular Engineering, Institute of Emergent Materials, Sogang University, Seoul 04107, Republic of Korea*

⁷*These authors contributed equally to this work*

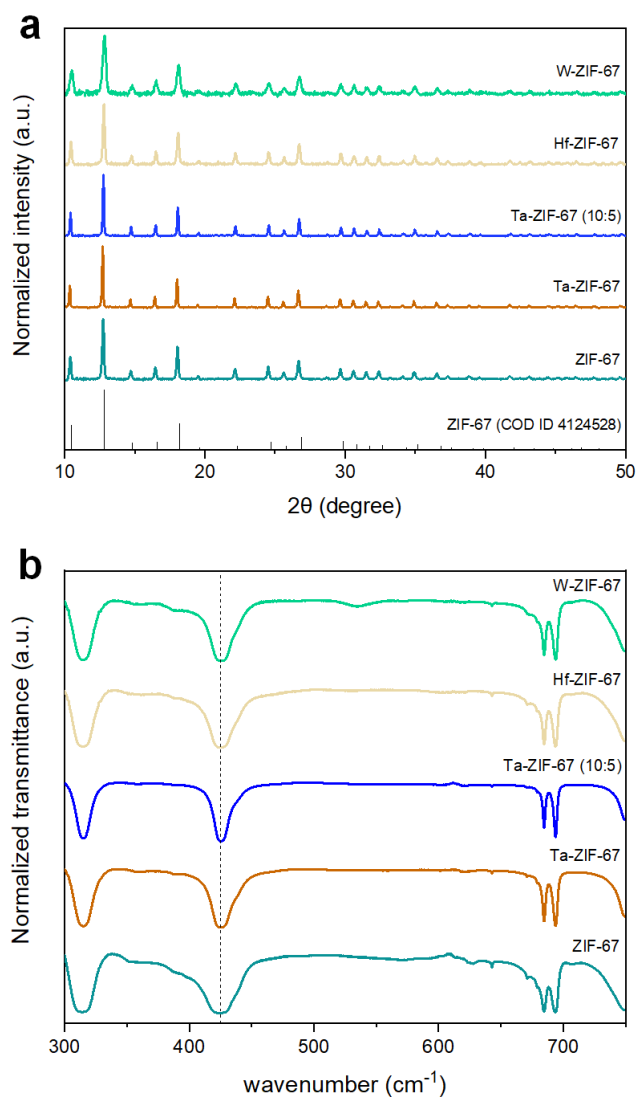


Figure S1. XRD patterns and IR spectra of various metal-doped ZIF-67 samples. (a) XRD patterns of Hf-ZIF-67, Ta-ZIF-67, W-ZIF-67 and ZIF-67. XRD pattern of Ta-ZIF-67 with increased Ta content is also shown (Ta-ZIF-67 (10:5)). (b) IR spectra of Hf-ZIF-67, Ta-ZIF-67, W-ZIF-67 and ZIF-67. An IR spectrum of ZIF-67 with increased Ta content is also shown. The dashed line indicates the peak corresponding to Co-N stretch vibration mode. According to the XRD and IR spectra, any variation of peaks wasn't observed after metal precursors were imprisoned in the ZIF-67, which implies the ZIF-67 maintained its crystal structure and no hetero metal species from metal precursors were formed.

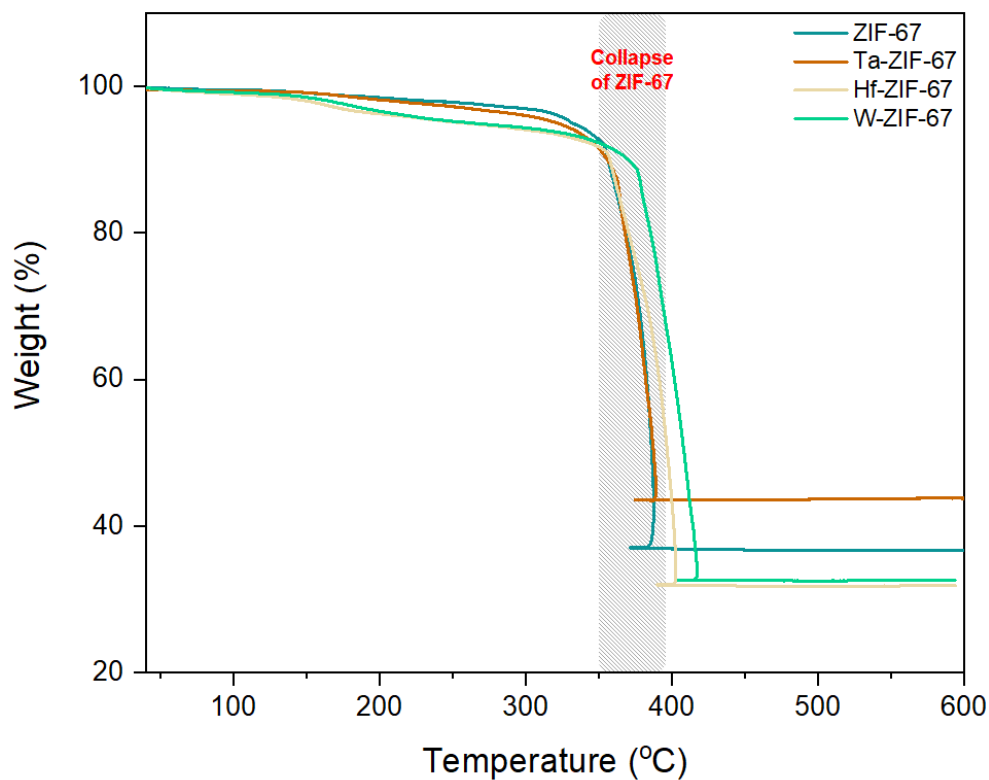


Figure S2. TGA of various metal-doped ZIF-67 samples. TGA for the ZIF-67, Ta-ZIF-67, Hf-ZIF-67, and W-ZIF-67. Ramping rate was 10 °C/min. Abrupt weight declination of samples was initiated before reaching 400 °C, which indicated that ZIF-67 structure was collapsed abruptly below 400 °C to isolate each hetero atom in the Co_3O_4 lattice as a single atom.

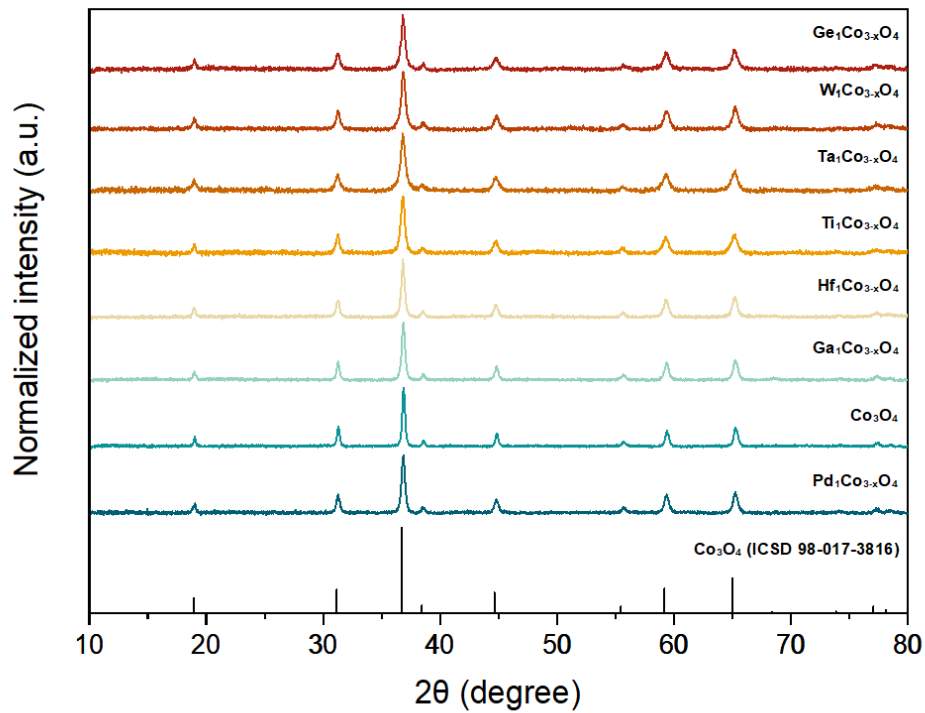


Figure S3. XRD patterns of $M_1Co_{3-x}O_4$ and Co_3O_4 . XRD patterns of $Pd_1Co_{3-x}O_4$, Co_3O_4 , $Ga_1Co_{3-x}O_4$, $Hf_1Co_{3-x}O_4$, $Ti_1Co_{3-x}O_4$, $Ta_1Co_{3-x}O_4$, $W_1Co_{3-x}O_4$, and $Ge_1Co_{3-x}O_4$. A standard XRD pattern of Co_3O_4 is displayed at the bottom. Peaks corresponding to the Co_3O_4 were only detected for all synthesized oxide samples.

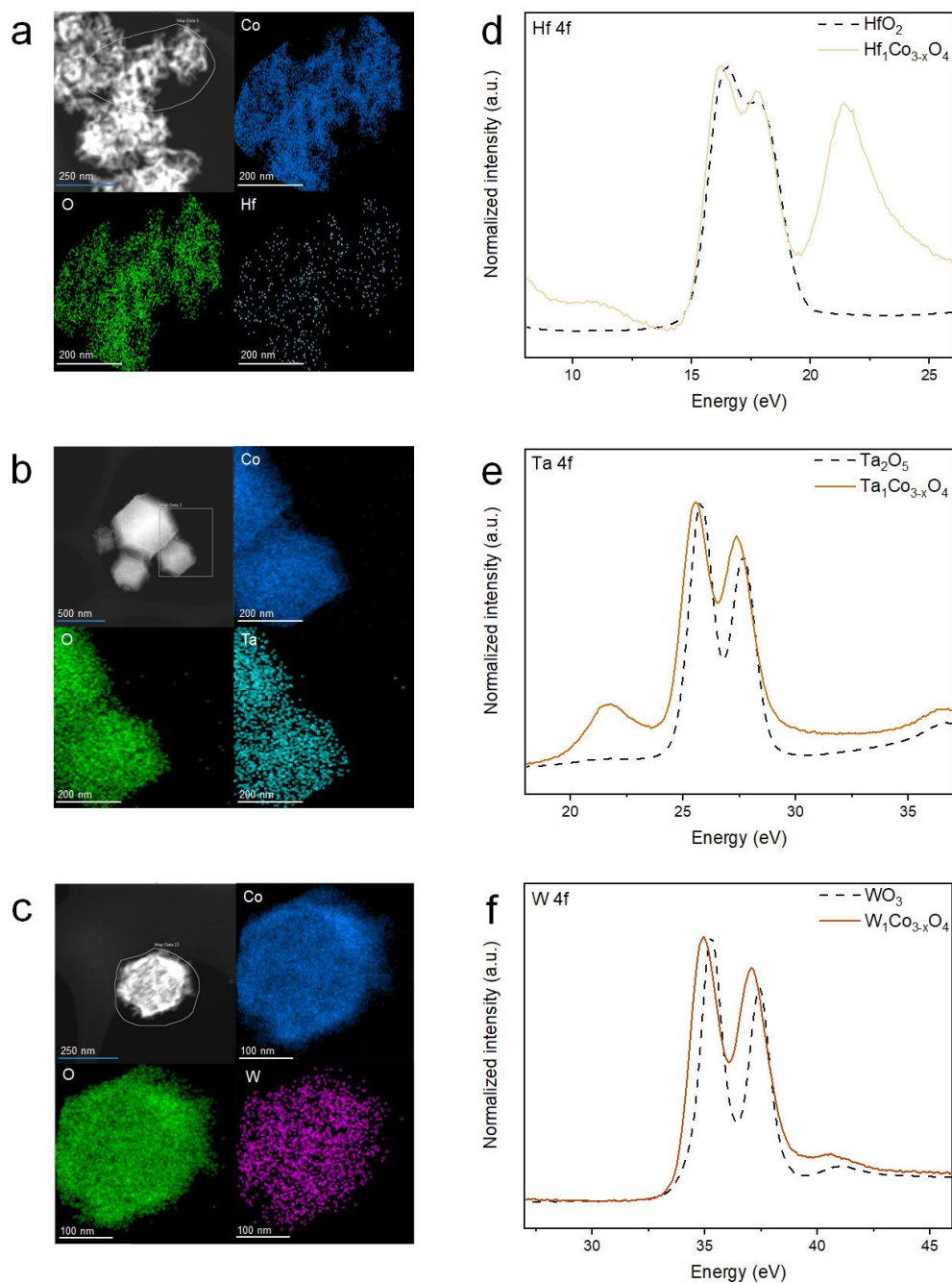


Figure S4. STEM-EDS mapping and XPS characterization of $\text{Hf}_1\text{Co}_{3-x}\text{O}_4$, $\text{Ta}_1\text{Co}_{3-x}\text{O}_4$, and $\text{W}_1\text{Co}_{3-x}\text{O}_4$. STEM images and corresponding EDS mapping of (a) $\text{Hf}_1\text{Co}_{3-x}\text{O}_4$, (b) $\text{Ta}_1\text{Co}_{3-x}\text{O}_4$, and (c) $\text{W}_1\text{Co}_{3-x}\text{O}_4$. EDS was conducted in the area bordered by a line shown in the STEM

images. EDS mapping revealed that metal atoms (Hf, Ta, W) were well dispersed within the cobalt oxide nanoparticles. 4f XPS spectra of (d) Hf, (e) Ta, and (f) W.

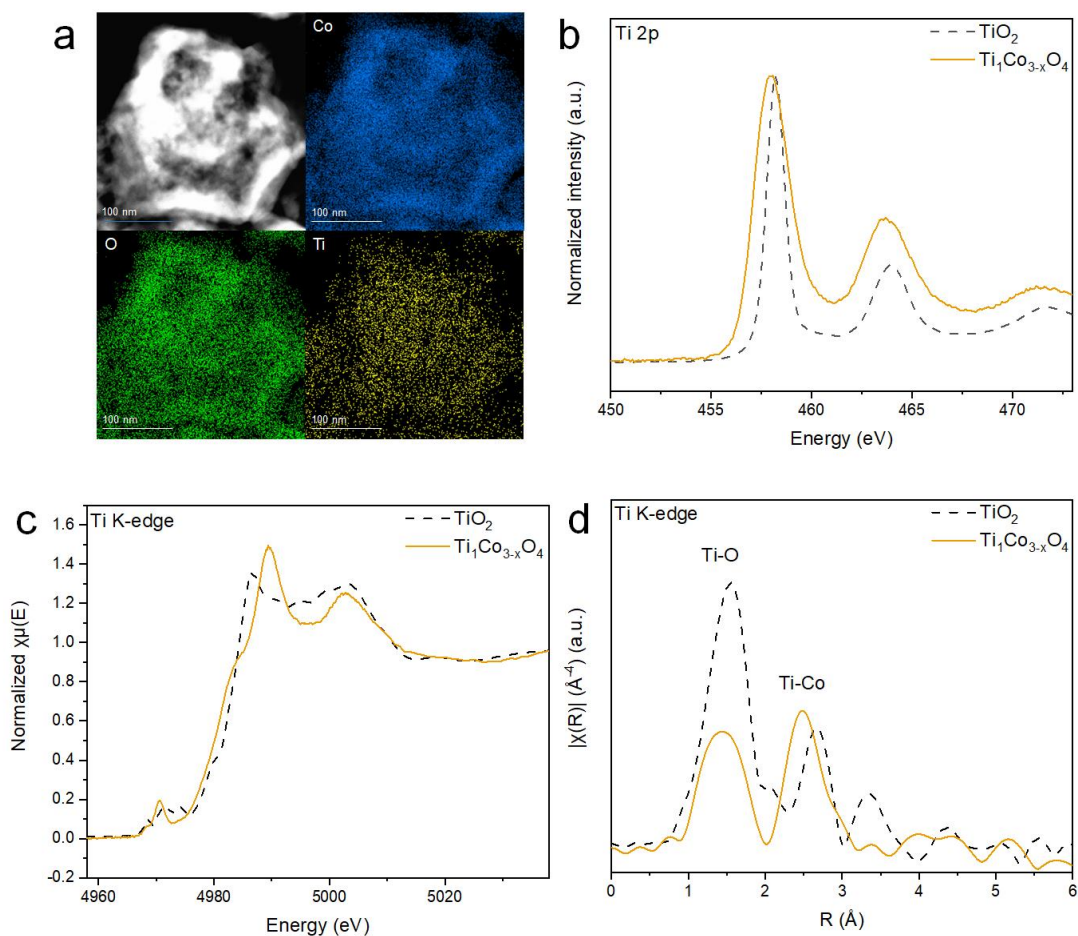


Figure S5. STEM-EDS mapping, XPS, XANES, and EXAFS characterization of $\text{Ti}_1\text{Co}_{3-x}\text{O}_4$.

(a) STEM image and the corresponding EDS mapping. EDS mapping revealed that Ti atoms were well dispersed within the cobalt oxide nanoparticles. (b) Ti 2p XPS spectra of $\text{Ti}_1\text{Co}_{3-x}\text{O}_4$ and TiO_2 (c) Ti K-edge XANES spectra of $\text{Ti}_1\text{Co}_{3-x}\text{O}_4$ and TiO_2 . (d) Ti K-edge EXAFS spectra of $\text{Ti}_1\text{Co}_{3-x}\text{O}_4$ and TiO_2 . EXAFS spectra demonstrated that Ti atoms are incorporated into Co_3O_4 lattice without aggregation or forming hetero TiO_2 phase.

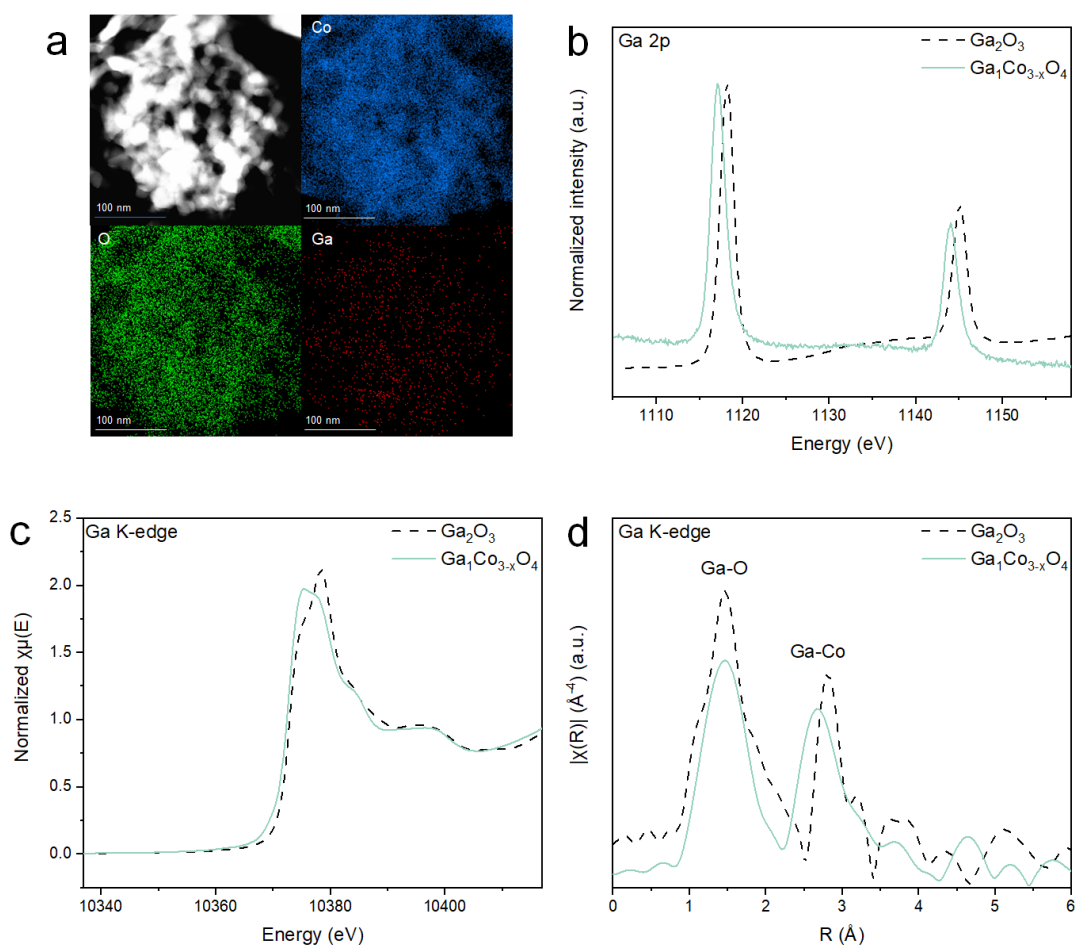


Figure S6. STEM-EDS mapping, XPS, XANES, and EXAFS characterization of $\text{Ga}_1\text{Co}_{3-x}\text{O}_4$.

(a) STEM image and the corresponding EDS mapping. EDS mapping revealed that Ga atoms were well dispersed within the cobalt oxide nanoparticles. (b) Ga 2p XPS spectra of $\text{Ga}_1\text{Co}_{3-x}\text{O}_4$ and Ga_2O_3 (c) Ga K-edge XANES spectra of $\text{Ga}_1\text{Co}_{3-x}\text{O}_4$ and Ga_2O_3 . (d) Ga K-edge EXAFS spectra of $\text{Ga}_1\text{Co}_{3-x}\text{O}_4$ and Ga_2O_3 . EXAFS spectra demonstrated that Ga atoms are incorporated into Co_3O_4 lattice without aggregation or forming hetero Ga_2O_3 phase.

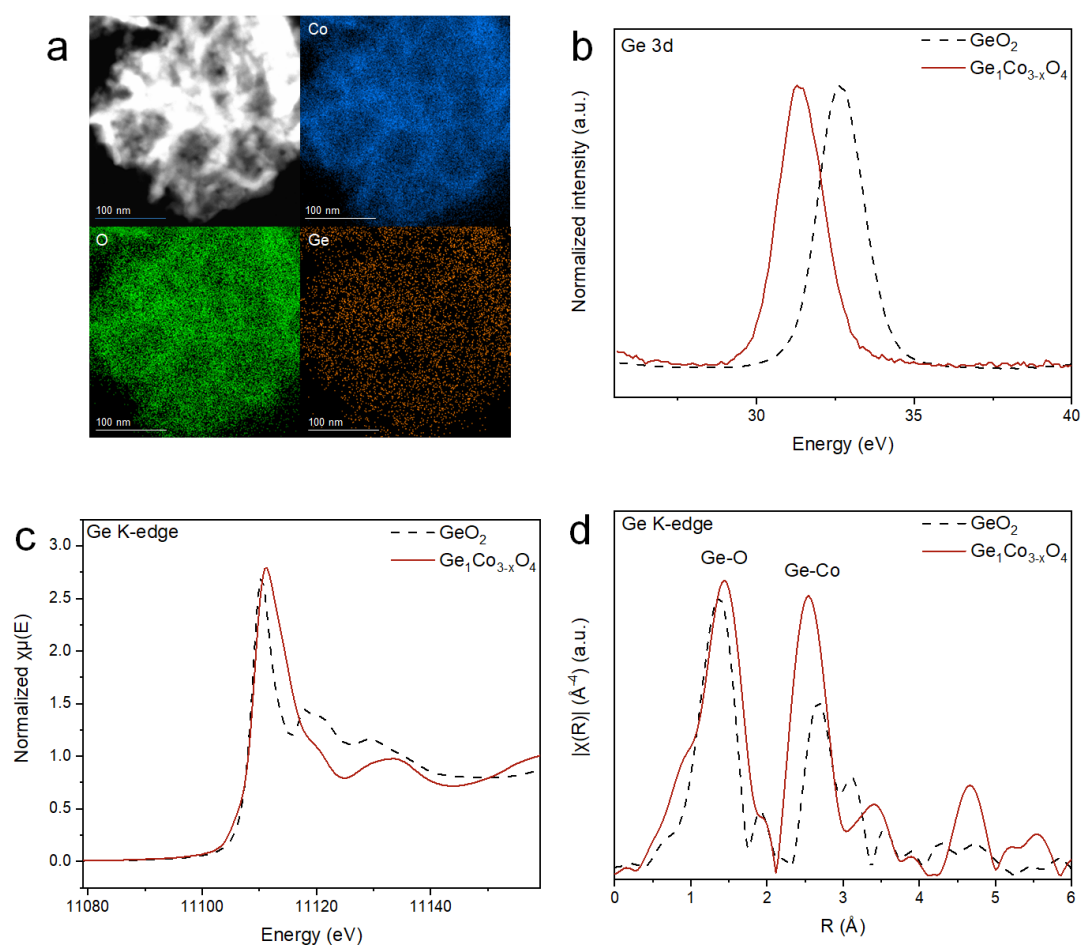


Figure S7. STEM-EDS mapping, XPS, XANES, and EXAFS characterization of $\text{Ge}_1\text{Co}_{3-x}\text{O}_4$.

(a) STEM image and the corresponding EDS mapping. EDS mapping revealed that Ge atoms were well dispersed within the cobalt oxide nanoparticles. (b) Ge 3d XPS spectra of $\text{Ge}_1\text{Co}_{3-x}\text{O}_4$ and GeO_2 (c) Ge K-edge XANES spectra of $\text{Ge}_1\text{Co}_{3-x}\text{O}_4$ and GeO_2 . (d) Ge K-edge EXAFS spectra of $\text{Ge}_1\text{Co}_{3-x}\text{O}_4$ and GeO_2 . EXAFS spectra demonstrated that Ge atoms are incorporated into Co_3O_4 lattice without aggregation or forming hetero GeO_2 phase.

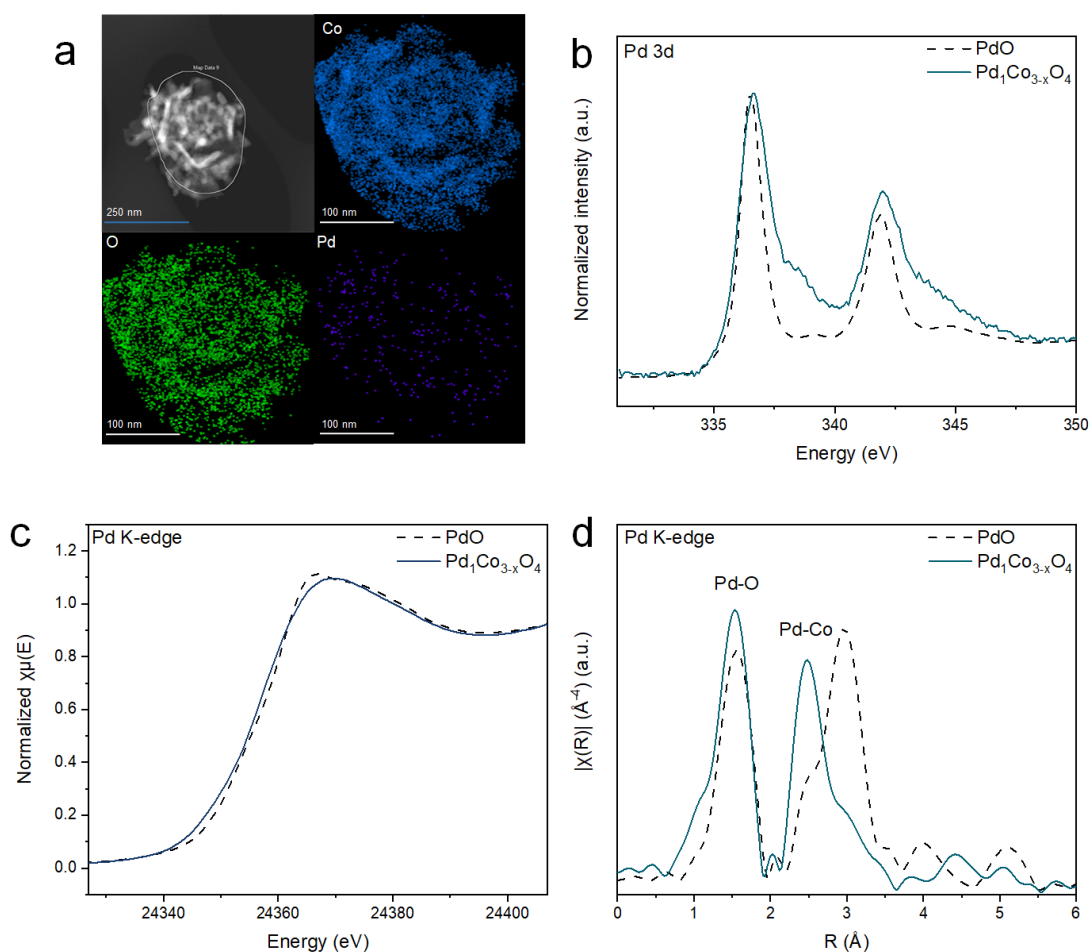


Figure S8. STEM-EDS mapping, XPS, XANES, and EXAFS characterization of $\text{Pd}_1\text{Co}_{3-x}\text{O}_4$.

(a) STEM image and the corresponding EDS mapping. EDS mapping revealed that Pd atoms were well dispersed within the cobalt oxide nanoparticles. (b) Pd 3d XPS spectra of $\text{Pd}_1\text{Co}_{3-x}\text{O}_4$ and PdO (c) Pd K-edge XANES spectra of $\text{Pd}_1\text{Co}_{3-x}\text{O}_4$ and PdO. (d) Pd K-edge EXAFS spectra of $\text{Pd}_1\text{Co}_{3-x}\text{O}_4$ and PdO. EXAFS spectra demonstrated that Pd atoms are incorporated into Co_3O_4 lattice without aggregation or forming hetero PdO phase.

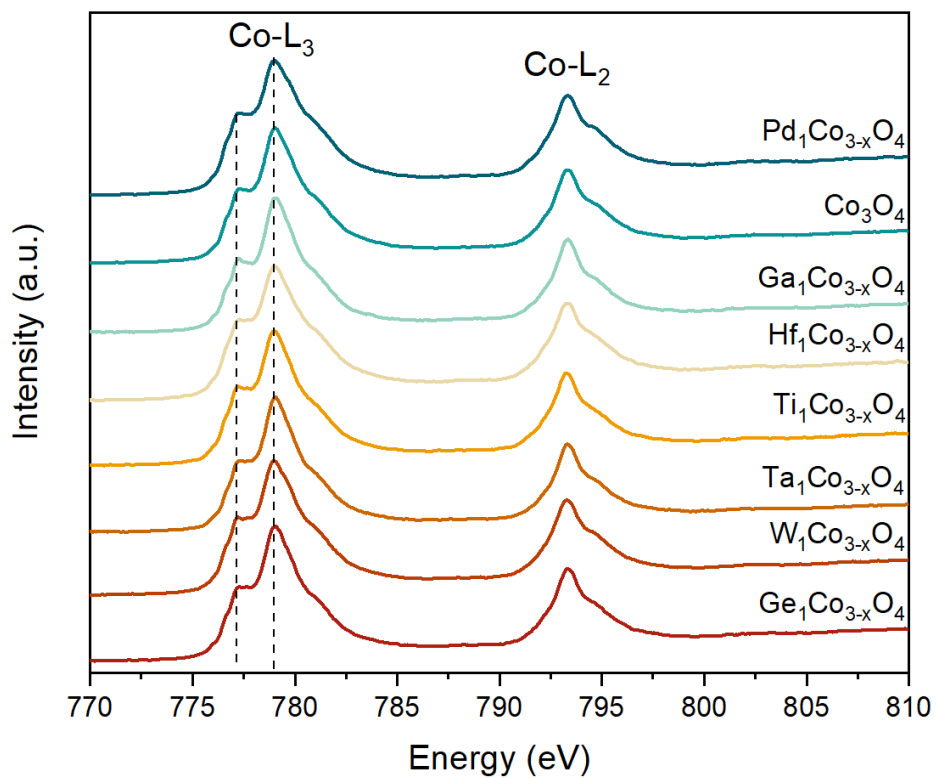


Figure S9. Co L-edge XAS of various metal doped CSO. The spectra of all the synthesized metal doped CSO have the same shape with the pristine CSO, indicating absence of alteration in surface structure after metal incorporation.

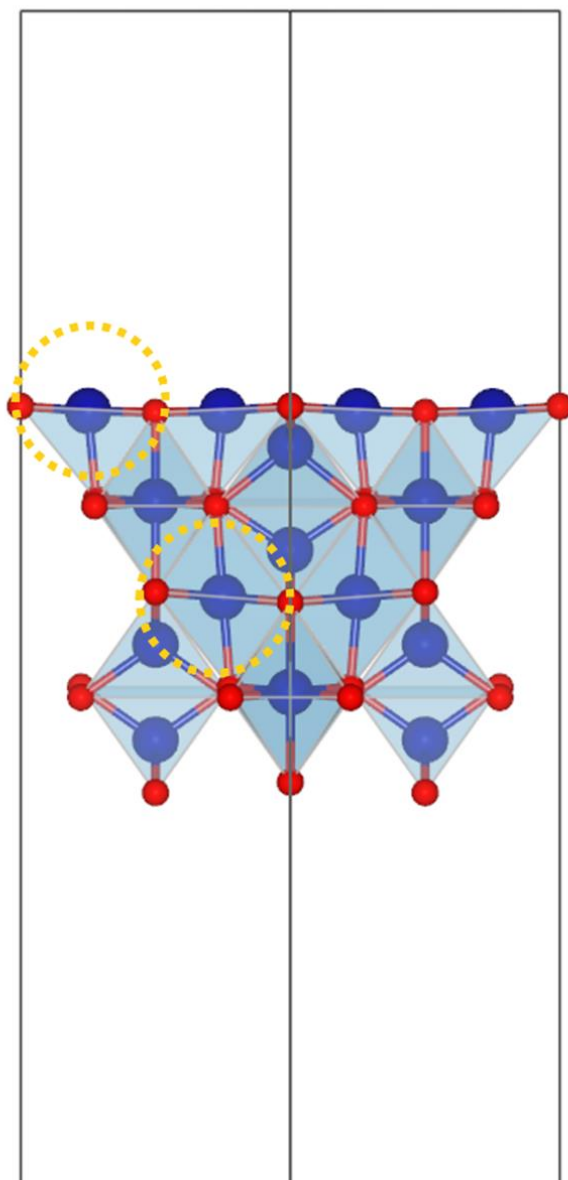


Figure S10. A side view of the atomic structure of the spinel Co_3O_4 (001) surface. Octahedral doping sites in the first and third layer are highlighted with dashed circles. Color codes: O (red), Co (blue).

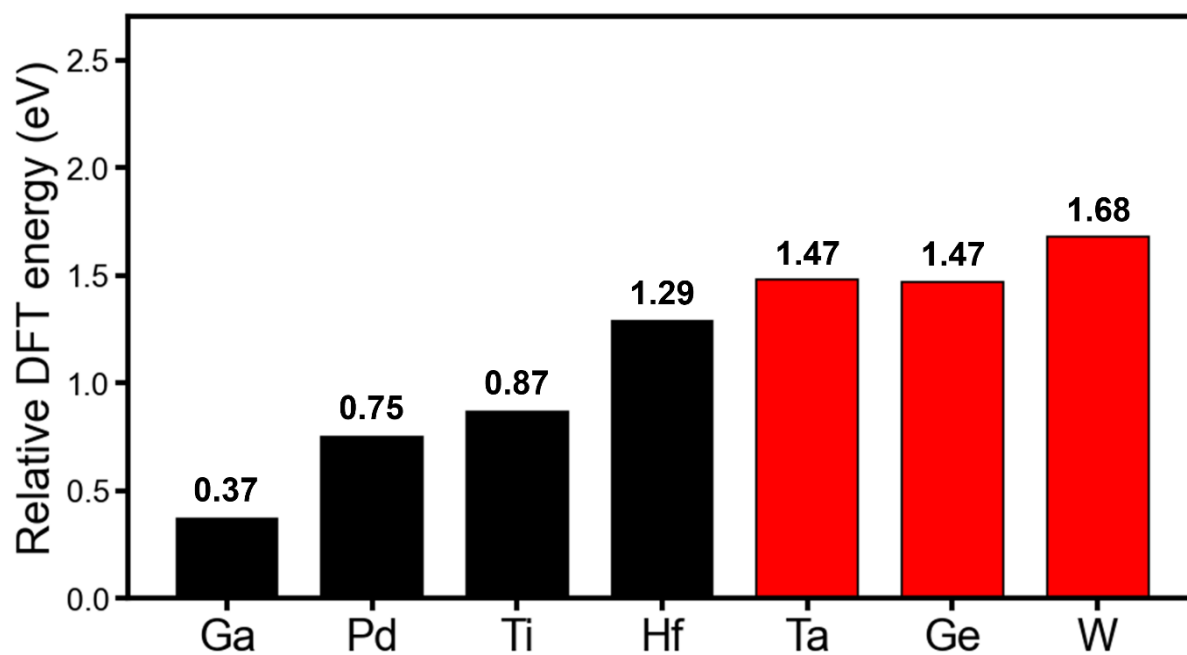


Figure S11. The relative DFT energy of metal dopants in the first layer (surface) with respect to the third layer (bulk) ($E_{\text{doped, 1st layer}} - E_{\text{doped, 3rd layer}}$), where more positive values suggest preferred surface location of dopants. Dopant metals observed on the surface in experiments are highlighted in red.

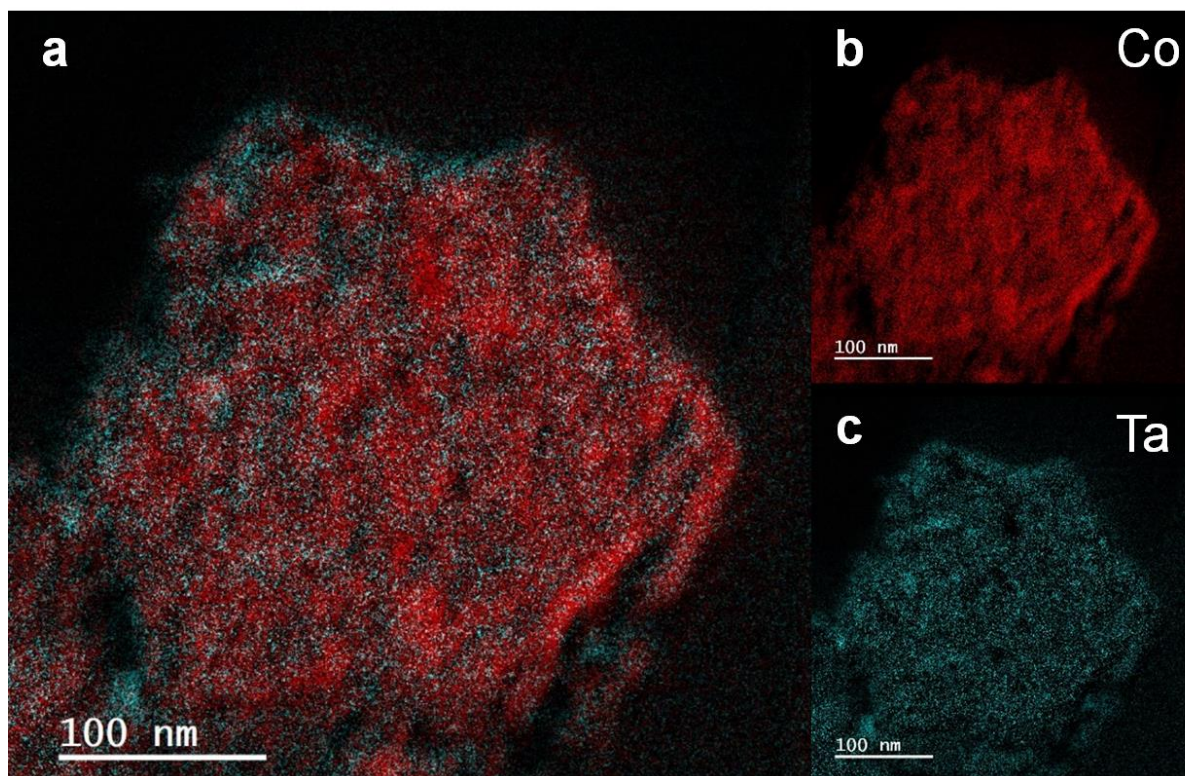


Figure S12. EF-TEM images of $\text{Ta}_1\text{Co}_{3-x}\text{O}_4$. (a) Cropped images of two EF-TEM images of (b) Co and (c) Ta. Cropped images showed that Ta atoms were dominantly located on the surface of the nanoparticle. Red indicates Co, sky blue indicates Ta.

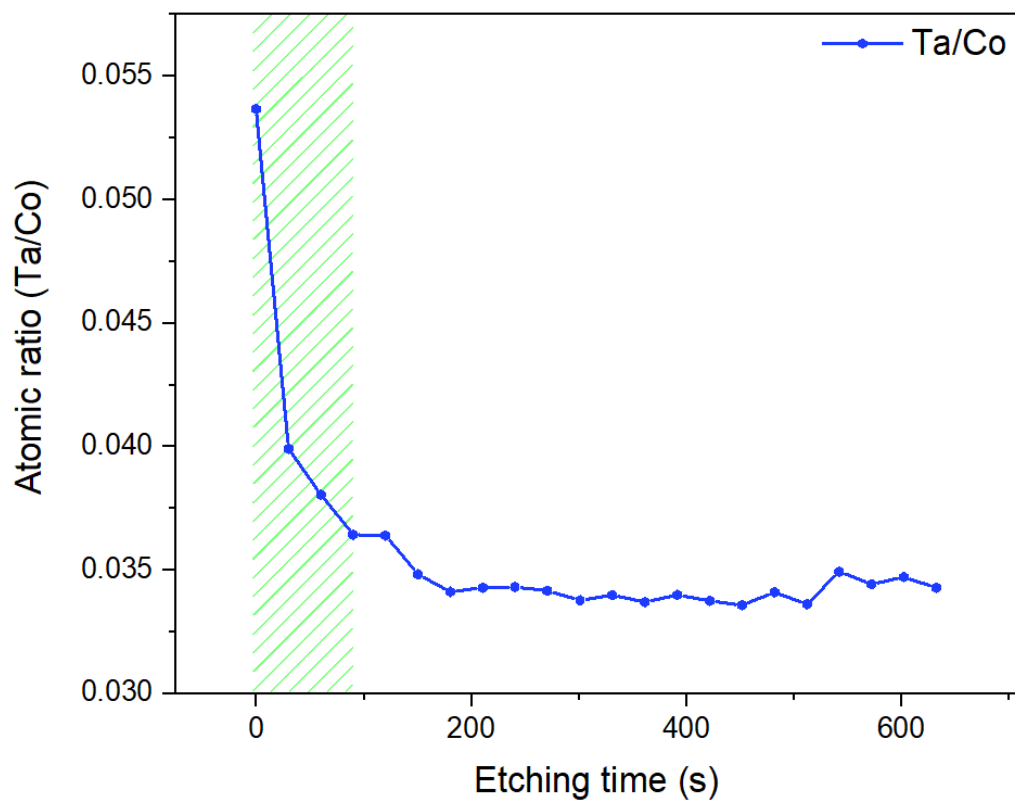


Figure S13. Ta/Co atomic ratio calculated by XPS depth profiling of $\text{Ta}_1\text{Co}_{3-x}\text{O}_4$. The Ta/Co atomic ratio gradually decreased over time, reaching a plateau profile. This suggests that Ta atoms are more likely to be stabilized on the surface.

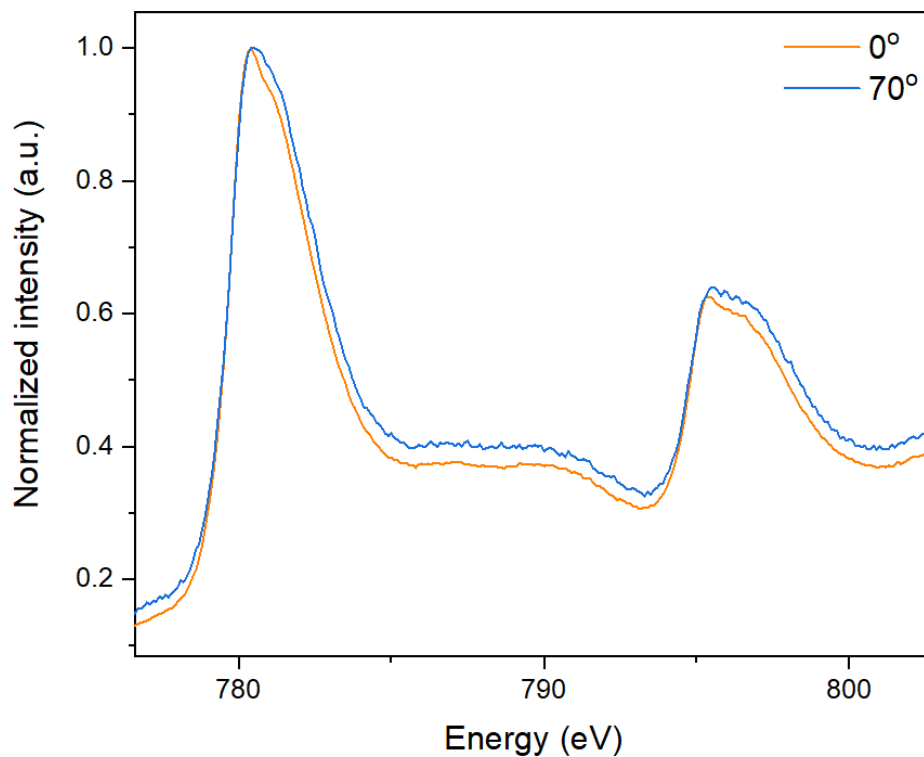


Figure S14. AR-XPS spectra of Ta₁Co_{3-x}O₄ nanoparticles. The degrees denote the incidence angle of X-ray to the sample. The graphs further revealed that the Co atoms closer to the surface tend to be more reduced. The tendency would be attributed to the higher Ta/Co ratio in the outer surface as Ta dopants would reduce the peripheral Co³⁺ to Co²⁺.

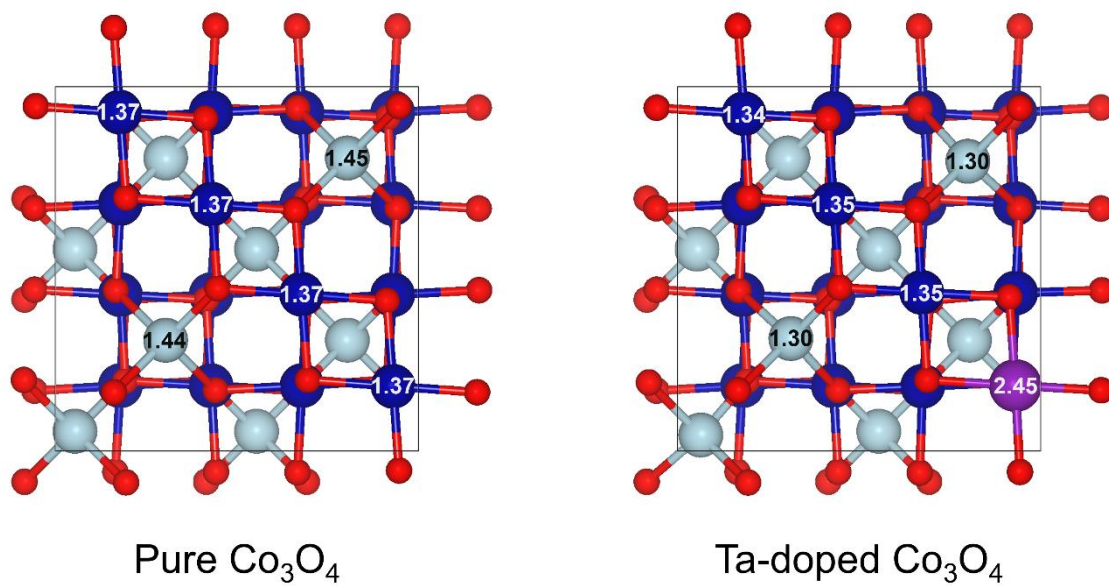


Figure S15. The Bader charges of the metal atoms in the 1st layer before and after Ta doping.
 Color codes: O (red), octahedral Co (blue), tetrahedral Co (skyblue), Ta (purple).

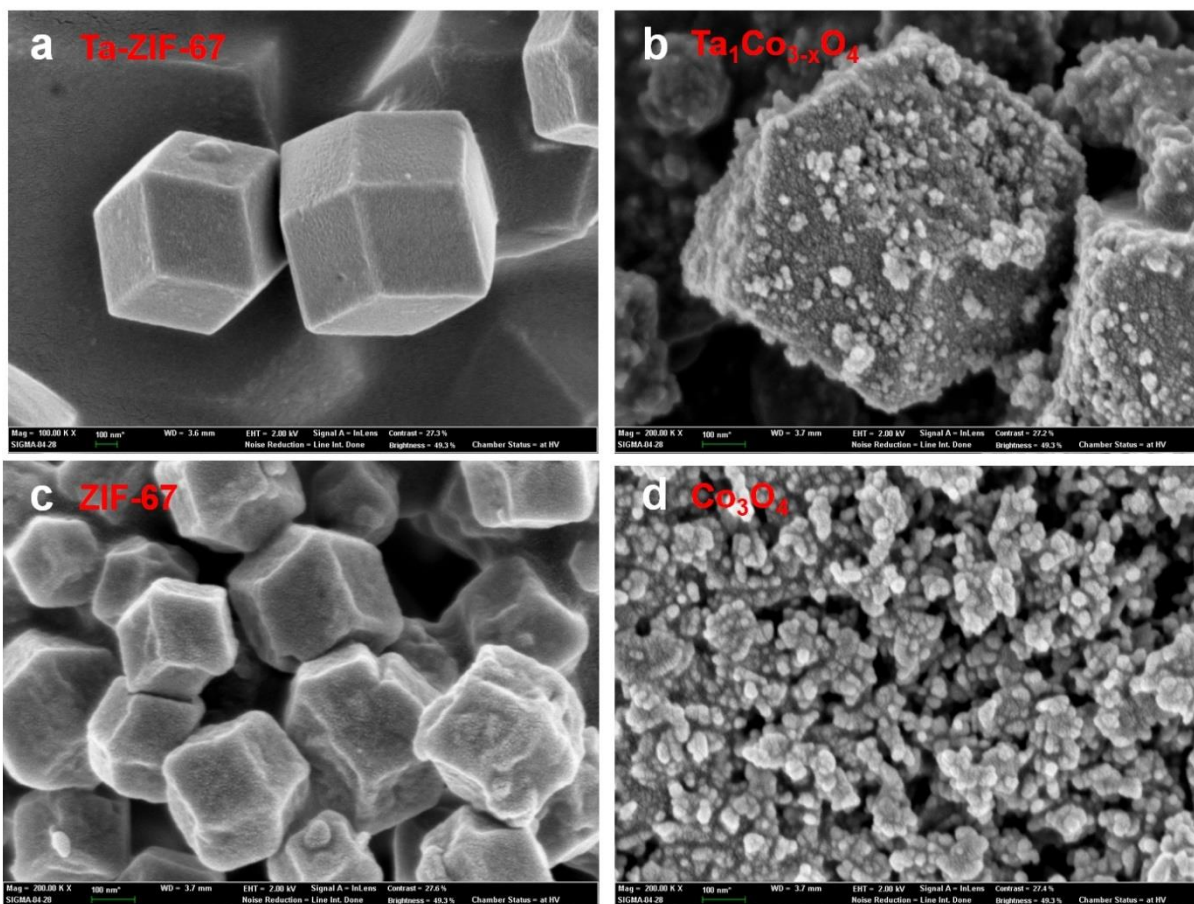


Figure S16. SEM images before and after calcination in air. SEM images of (a) Ta-ZIF-67 and (b) Ta₁Co_{3-x}O₄. SEM images of (c) ZIF-67 and (d) Co₃O₄. Without any hetero metal incorporation, ZIF structure is shown to be collapsed after calcination.

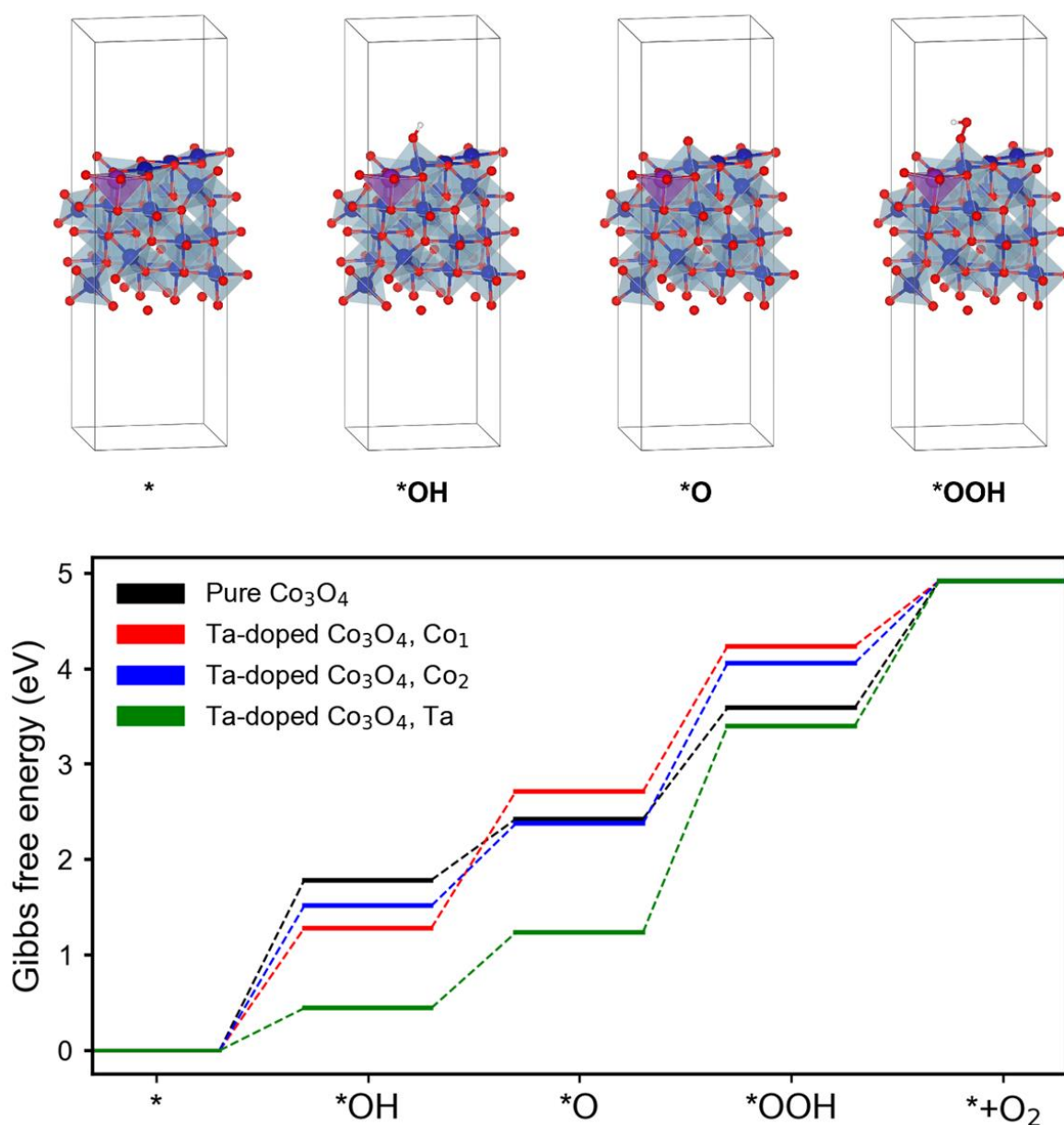


Figure S17. (Top) Optimized structures of OER intermediates. **(Bottom)** The Gibbs free energy diagram of updoped and Ta-doped Co₃O₄. For Ta-doped Co₃O₄, we considered three distinct adsorption sites, i.e., Co sites close to and far from Ta, and Ta site. Color codes: O (red), H (white), Co (blue), Ta (purple).

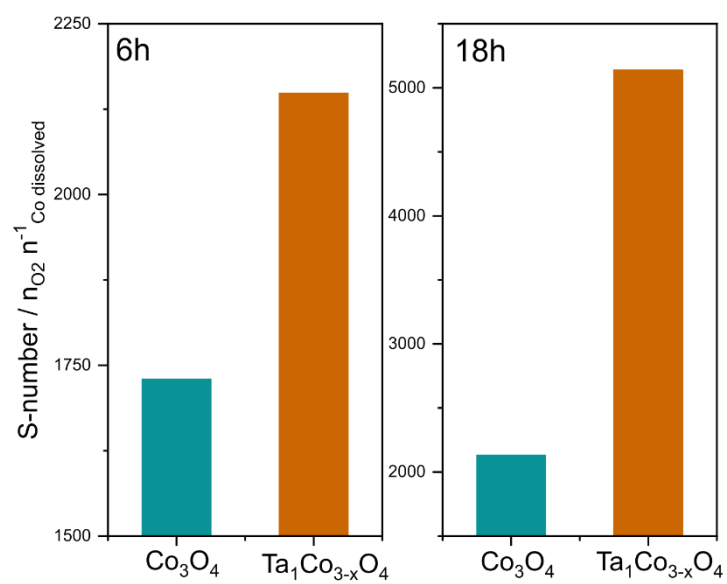


Figure S18. Calculation of S-number. The Bar graphs illustrate the S-number for Ta₁Co_{3-x}O₄ and Co₃O₄ at 6 hours (left) and 18 hours (right).

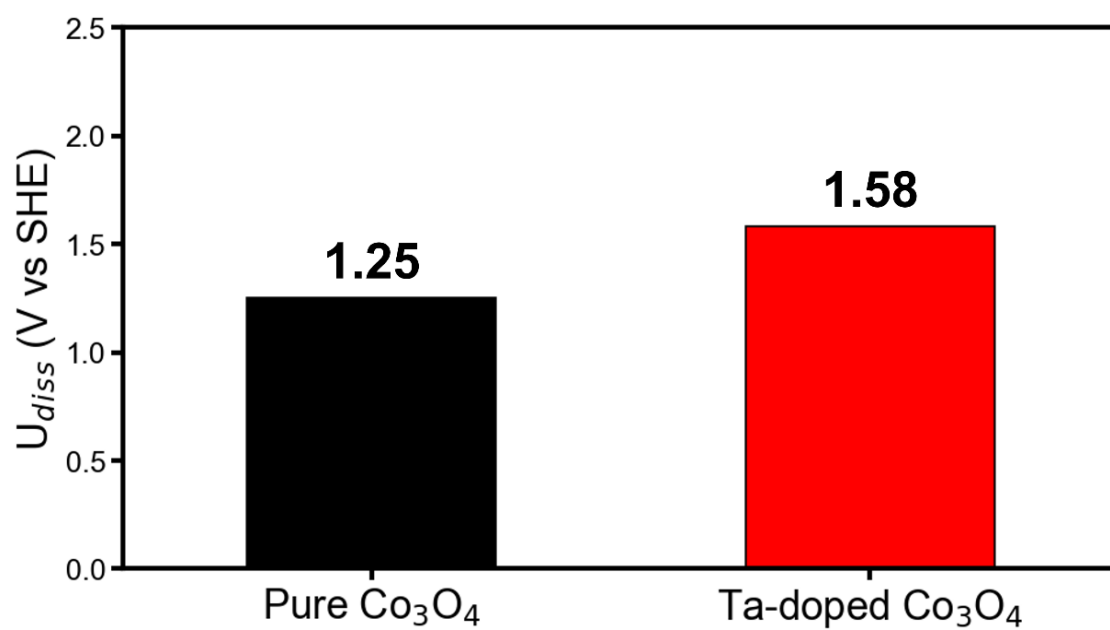


Figure S19. Dissolution potentials (U_{diss}) of tetrahedral Co atoms from slab structures.

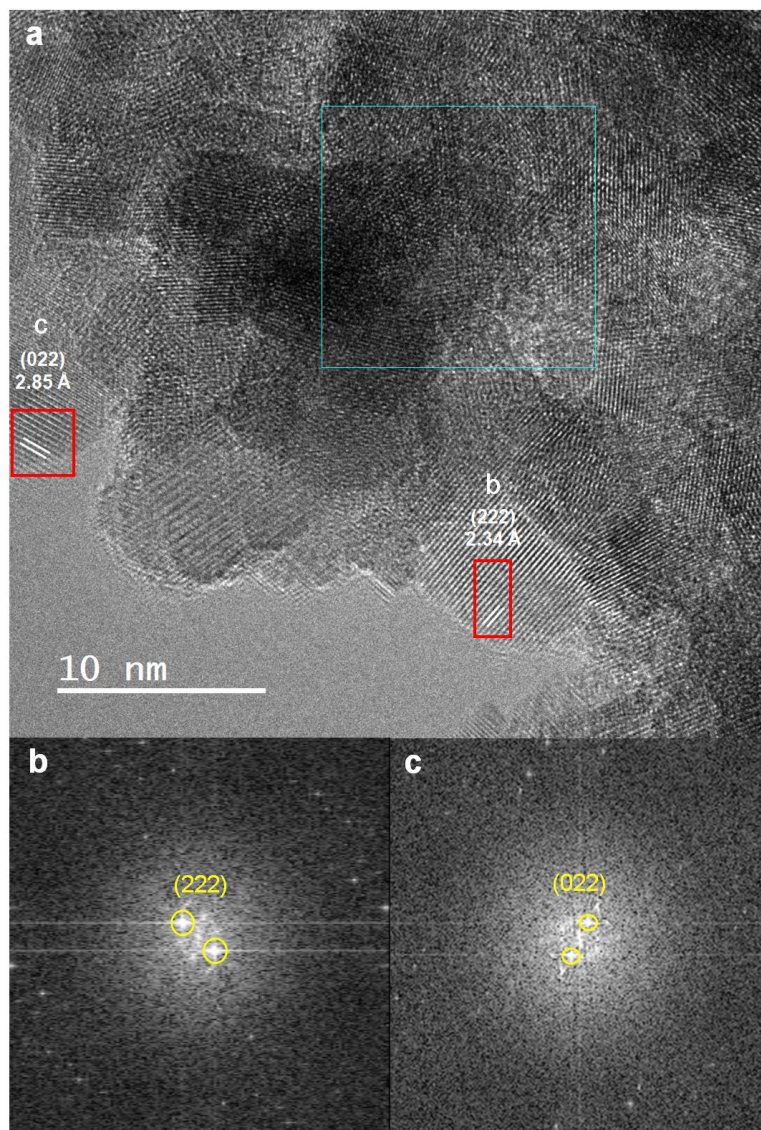


Figure S20. CS-TEM image of $\text{Ta}_1\text{Co}_{3-x}\text{O}_4$ after OER and FFT patterns. (a) CS-TEM image of $\text{Ta}_1\text{Co}_{3-x}\text{O}_4$ after OER. Lattice bordered by the red lines indicated (022) and (222) planes of Co_3O_4 maintained after acidic OER without forming amorphous phase respectively. The catalyst was not suffered from forming new structures near the surfaces after OER. The cyan border line just indicates that drift correction was conducted during the image acquisition. FFT pattern of (b) (222) planes and (c) (022) planes corresponding to the red border line in (a).

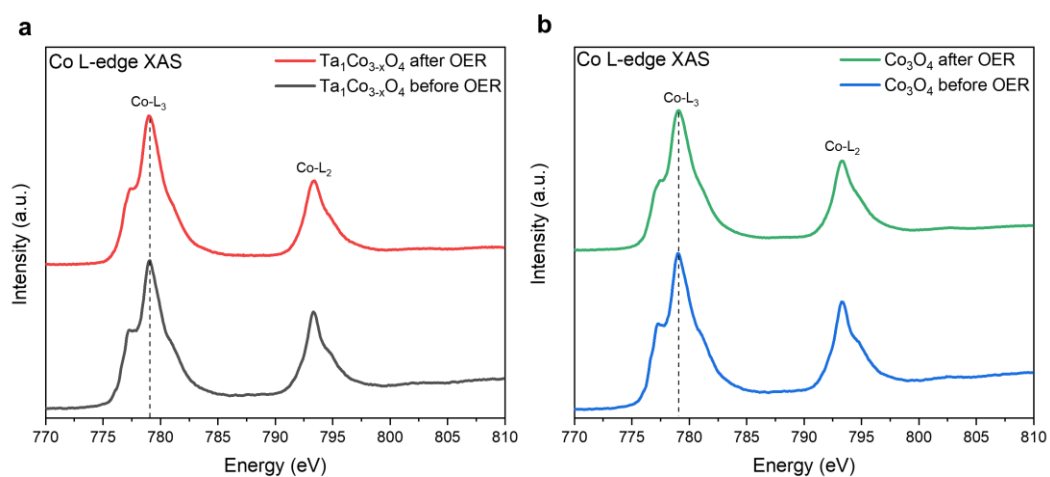


Figure S21. (a) Co L-edge XAS spectra of $\text{Ta}_1\text{Co}_{3-x}\text{O}_4$ before and after OER. (b) Co L-edge XAS spectra of Co_3O_4 before and after OER. It is evident that the spectra of $\text{Ta}_1\text{Co}_{3-x}\text{O}_4$ after OER share the same shape as the one before OER, indicating an absence of alteration in the surface structure during the reaction.

Table S1. Peaks used for deconvolution of Co 2P XPS peaks and results of the XPS fitting.

Co_3O_4	Name	Position (eV)	FWHM	Area (%)	$\text{Pd}_2\text{Co}_{3-x}\text{O}_4$	Name	Position (eV)	FWHM	Area (%)
1	$\text{Co}^{3+} 2p_{3/2}$	779.17	1.785	27.44870032	1	$\text{Co}^{3+} 2p_{3/2}$	779.217	1.574	24.89083
2	$\text{Co}^{3+} 2p_{1/2}$	794.575	2.054	13.72435507	2	$\text{Co}^{3+} 2p_{1/2}$	794.459	1.76	12.44541
3	$\text{Co}^{2+} 2p_{3/2}$	780.502	2.669	26.448889	3	$\text{Co}^{2+} 2p_{3/2}$	780.509	2.546	23.87596
4	$\text{Co}^{2+} 2p_{1/2}$	796.473	2.435	13.22444941	4	$\text{Co}^{2+} 2p_{1/2}$	796.251	2.558	11.93798
5	$\text{Co}^{3+} 2p_{3/2}$ satellite	783.252	4.5	8.64547263	5	$\text{Co}^{3+} 2p_{3/2}$ satellite	783	4.5	11.78109
6	$\text{Co}^{2+} 2p_{3/2}$ satellite	788.556	3.566	4.486803951	6	$\text{Co}^{2+} 2p_{3/2}$ satellite	788.231	4.427	7.477051
7	$\text{Co}^{3+} 2p_{1/2}$ satellite	802.1	3.106	1.555324074	7	$\text{Co}^{3+} 2p_{1/2}$ satellite	800.21	4	2.000642
8	$\text{Co}^{2+} 2p_{1/2}$ satellite	804.543	4.18	4.466005539	8	$\text{Co}^{2+} 2p_{1/2}$ satellite	804.011	4.5	5.59103
$\text{Ga}_1\text{Co}_{3-x}\text{O}_4$	Name	Position (eV)	FWHM	Area (%)	$\text{Hf}_2\text{Co}_{3-x}\text{O}_4$	Name	Position (eV)	FWHM	Area (%)
1	$\text{Co}^{3+} 2p_{3/2}$	779.29	1.77	23.7136	1	$\text{Co}^{3+} 2p_{3/2}$	779.356	1.765	23.2296
2	$\text{Co}^{3+} 2p_{1/2}$	794.39	1.74	11.8568	2	$\text{Co}^{3+} 2p_{1/2}$	794.522	1.833	11.6148
3	$\text{Co}^{2+} 2p_{3/2}$	780.54	2.73	24.78196	3	$\text{Co}^{2+} 2p_{3/2}$	780.729	2.839	25.0189
4	$\text{Co}^{2+} 2p_{1/2}$	796.156	2.805	12.39098	4	$\text{Co}^{2+} 2p_{1/2}$	796.291	3.103	12.50945
5	$\text{Co}^{3+} 2p_{3/2}$ satellite	783.2	4.5	11.6561	5	$\text{Co}^{3+} 2p_{3/2}$ satellite	784.024	4.5	11.20693
6	$\text{Co}^{2+} 2p_{3/2}$ satellite	788.341	4.45	7.810653	6	$\text{Co}^{2+} 2p_{3/2}$ satellite	788.718	4.244	7.992647
7	$\text{Co}^{3+} 2p_{1/2}$ satellite	801	4.5	3.069326	7	$\text{Co}^{3+} 2p_{1/2}$ satellite	801.5	4.5	3.891565
8	$\text{Co}^{2+} 2p_{1/2}$ satellite	804.385	4.363	4.720573	8	$\text{Co}^{2+} 2p_{1/2}$ satellite	804.729	4.442	4.5361
$\text{Ti}_1\text{Co}_{3-x}\text{O}_4$	Name	Position (eV)	FWHM	Area (%)	$\text{Ta}_1\text{Co}_{3-x}\text{O}_4$	Name	Position (eV)	FWHM	Area (%)
1	$\text{Co}^{3+} 2p_{3/2}$	779.453	1.954	21.47878	1	$\text{Co}^{3+} 2p_{3/2}$	779.613	1.778	19.38957
2	$\text{Co}^{3+} 2p_{1/2}$	794.553	1.948	10.73939	2	$\text{Co}^{3+} 2p_{1/2}$	794.613	1.74	9.694783
3	$\text{Co}^{2+} 2p_{3/2}$	780.732	3.062	26.66217	3	$\text{Co}^{2+} 2p_{3/2}$	780.852	3.11	28.02924
4	$\text{Co}^{2+} 2p_{1/2}$	796.351	2.817	13.33109	4	$\text{Co}^{2+} 2p_{1/2}$	796.368	3.127	14.01462
5	$\text{Co}^{3+} 2p_{3/2}$ satellite	784.059	4.5	11.62416	5	$\text{Co}^{3+} 2p_{3/2}$ satellite	784.467	4.5	11.04615
6	$\text{Co}^{2+} 2p_{3/2}$ satellite	788.501	4.452	7.993419	6	$\text{Co}^{2+} 2p_{3/2}$ satellite	788.933	4.392	8.633043
7	$\text{Co}^{3+} 2p_{1/2}$ satellite	801	4.832	2.955508	7	$\text{Co}^{3+} 2p_{1/2}$ satellite	801.5	4.5	4.220017
8	$\text{Co}^{2+} 2p_{1/2}$ satellite	804.23	4.5	5.215483	8	$\text{Co}^{2+} 2p_{1/2}$ satellite	804.814	4.502	4.972582
$\text{W}_1\text{Co}_{3-x}\text{O}_4$	Name	Position (eV)	FWHM	Area (%)	$\text{Ge}_1\text{Co}_{3-x}\text{O}_4$	Name	Position (eV)	FWHM	Area (%)
1	$\text{Co}^{3+} 2p_{3/2}$	779.539	1.697	18.63505	1	$\text{Co}^{3+} 2p_{3/2}$	779.678	1.817	18.65094
2	$\text{Co}^{3+} 2p_{1/2}$	794.822	1.916	9.317526	2	$\text{Co}^{3+} 2p_{1/2}$	794.678	1.701	9.325465
3	$\text{Co}^{2+} 2p_{3/2}$	780.763	2.978	29.89663	3	$\text{Co}^{2+} 2p_{3/2}$	780.735	3.114	30.13371
4	$\text{Co}^{2+} 2p_{1/2}$	796.666	2.807	14.94831	4	$\text{Co}^{2+} 2p_{1/2}$	796.325	2.928	15.06685
5	$\text{Co}^{3+} 2p_{3/2}$ satellite	784	4.5	13.22573	5	$\text{Co}^{3+} 2p_{3/2}$ satellite	784.021	4.5	10.93358
6	$\text{Co}^{2+} 2p_{3/2}$ satellite	788.551	4.242	6.208046	6	$\text{Co}^{2+} 2p_{3/2}$ satellite	788.779	4.315	7.136013
7	$\text{Co}^{3+} 2p_{1/2}$ satellite	801.2	4.407	2.029593	7	$\text{Co}^{3+} 2p_{1/2}$ satellite	800.802	4.5	3.095454
8	$\text{Co}^{2+} 2p_{1/2}$ satellite	804.242	4.5	5.739109	8	$\text{Co}^{2+} 2p_{1/2}$ satellite	804.598	4.5	5.657994

Table S2. Surface composition (Co, M, O) and M/Co ratio (%) of different $M_1Co_{3-x}O_4$ measured by XPS.

Catalyst	Co at.%	M at.%	O at.%	M/Co Ratio (%)
$Pd_1Co_{3-x}O_4$	34.23	1.36	64.41	3.97
$Ga_1Co_{3-x}O_4$	31.37	2.94	65.69	9.37
$Hf_1Co_{3-x}O_4$	34.13	1.01	64.86	2.96
$Ti_1Co_{3-x}O_4$	30.61	4.78	64.61	15.6
$Ta_1Co_{3-x}O_4$	31.33	4.24	64.43	13.5
$W_1Co_{3-x}O_4$	28.21	4.00	67.79	14.2
$Ge_1Co_{3-x}O_4$	29.34	5.98	64.68	20.4

* Various metal dopants were designated as M

Table S3. Co and M concentration (ppm) of different $M_1Co_{3-x}O_4$ obtained from ICP-AES measurement. Co and M Atomic percent and M/Co ratio (%) were calculated.

Catalyst	Sample mass (mg)	Co Concentration (ppm)	M Concentration (ppm)	M wt. %	Co at. %	M at. %	M/Co ratio (%)
$Pd_1Co_{3-x}O_4$	7.4	1846.97	53.46	3.61	98.42	1.58	1.61
$Ga_1Co_{3-x}O_4$	6.4	1383.90	56.23	4.39	96.68	3.32	3.43
$Hf_1Co_{3-x}O_4$	7.1	946.37	41.87	2.95	98.56	1.44	1.46
$Ti_1Co_{3-x}O_4$	8.1	1124.61	58.37	3.60	93.98	6.02	6.41
$Ta_1Co_{3-x}O_4$	7.2	880.77	85.29	5.92	96.94	3.06	3.16
$W_1Co_{3-x}O_4$	23.0	1494.19	123.24	5.36	97.42	2.58	2.65
$Ge_1Co_{3-x}O_4$	21.0	1456.85	63.88	3.04	96.57	3.43	3.55

* Various metal dopants were designated as M

Table S4. Co and Ta concentration (ppm) of $\text{Ta}_1\text{Co}_{3-x}\text{O}_4$ with varying Ta amount in the synthetic step obtained from ICP-AES measurement.

Catalyst	Sample mass (mg)	Co Concentration (ppm)	Ta Concentration (ppm)	Ta wt. %	Co at. %	Ta at. %	Ta/Co ratio (%)
$\text{Ta}_1\text{Co}_{3-x}\text{O}_4$ (10:1)	7.3	980.26	42.48	2.91	98.61	1.39	1.41
$\text{Ta}_1\text{Co}_{3-x}\text{O}_4$	7.2	880.77	85.29	5.92	96.94	3.06	3.16
$\text{Ta}_1\text{Co}_{3-x}\text{O}_4$ (10:5)	11.1	146.71	22.84	10.29	95.17	4.83	5.08

Table S5. Comparison of stability and activity of our Ta₁Co_{3-x}O₄ with reported cobalt spinel oxide structure based acidic OER electrocatalyst.

Catalysts	Electrolyte	Stability	η (mV) at 10 mA cm ⁻²	Reference
Ta ₁ Co _{3-x} O ₄	0.05 M H ₂ SO ₄	140 h @ 10 mA cm ⁻²	378	This work
Ag-Co ₃ O ₄ nanosheets	0.5 M H ₂ SO ₄	1000 CV	470	<i>J. Mater. Chem. A</i> , 6 , 5678-5686 (2018)
Co ₃ O ₄ /CeO ₂	0.5 M H ₂ SO ₄	50 h @ 10 mA cm ⁻²	423	<i>Nat. Commun.</i> 12 , 3036 (2021)
Co ₂ TiO ₄	0.5 M H ₂ SO ₄	10 h @ 10 ~ 5 mA cm ⁻²	513	<i>ACS Catal.</i> 7 , 4, 2770–2779 (2017)
Co ₃ O ₄ film	0.5 M H ₂ SO ₄	12 h @ 10 mA cm ⁻²	570	<i>Chem. Mater.</i> 29 , 3, 950–957 (2017)
Na-treated Mesoporous Co ₃ O ₄	0.5 M H ₂ SO ₄	9 h @ 10 mA cm ⁻²	412	<i>Nat. Commun.</i> 13 , 7754 (2022)
Li 5 at% Co ₃ O ₄ thin film	0.05 M H ₂ SO ₄	15 h @ mA cm ⁻²	510	<i>ChemCatChem</i> , 13 , 1, 459-467 (2021)
FeCo ₂ O ₄	0.5 M H ₂ SO ₄	N/A	>570	<i>IOP Conf. Ser.: Mater. Sci. Eng.</i> 872 , 012182
Co ₃ O ₄ @C/GPO composite	1 M H ₂ SO ₄	43 h @ mA cm ⁻²	360	<i>Nat. Commun.</i> 13 , 4341 (2022)